



Experimental Study of the Effects of Borehole Size, Borehole Roughness, and Installation Pressure on the Pull Load Capacity of Inflatable Rockbolts

Charlie C. Li¹ · Andreas Aure^{1,3} · Greig Knox²

Received: 14 February 2023 / Accepted: 25 July 2023 / Published online: 20 August 2023
© The Author(s) 2023

Abstract

An inflatable rockbolt is a steel tube that has been rolled into an omega shape. During installation, water is injected into the tube, which expands the profile of the rockbolt, generating a radial force against the borehole wall. This reinforces the rock mass through the friction at the bolt–rock interface. This study aims to quantify the effects of borehole size, borehole roughness, and installation water pressure on the pull load capacity of the bolt. This was achieved through a series of pull tests under laboratory conditions. The test results showed that the load capacity was higher in boreholes that were either close to the initial profile diameter of the bolt or the fully unfolded diameter of the bolt, that were 26.8 mm and 38.7 mm, respectively, in the study. The load capacity and the radial stiffness of the bolt were lowest in the medium-sized boreholes (33 and 33.5 mm). In small boreholes, the shoulders of the bolt tongue are tightly compressed such that the outward elastic deformation of the bolt tube is locked in after installation. This deformation locking enhances the load capacity of the bolt. In addition, the load capacity was found to be higher in percussively drilled boreholes than in diamond-drilled boreholes. The additional friction angle of the percussive boreholes was back-calculated to be approximately 5.83° . The load capacity was also found to increase as the installation water pressure increases in the range of pressures tested. It was observed that the inflatable bolt was clamped against the borehole in three zones: on the two tongue shoulders and the side of the bolt opposite the tongue.

Highlights

- The pull load of an inflatable bolt is minimum as the borehole diameter is in the middle of the initial and fully unfolded diameters of the bolt.
- In small boreholes, the clamping of the shoulders of the tube tongue results in higher contact stress and consequently higher pull load capacities.
- Borehole roughness is vital in enhancing the pull load capacity of inflatable bolt. The roughness angle of a percussive borehole is around 5.83° .
- The pull load capacity of the inflatable bolts increased as the installation water pressure increased from 24 to 30 MPa.
- An installed inflatable bolt contacts the borehole at the two tongue shoulders and in a zone around the opposite of the tongue.

Keywords Inflatable rockbolt · Pullout test · Borehole size · Roughness · Installation water pressure

✉ Charlie C. Li
Charlie.c.li@ntnu.no

¹ Department of Geoscience and Petroleum, NTNU
Norwegian University of Science and Technology,
Trondheim, Norway

² Epiroc, Johannesburg, South Africa

³ Present Address: Multiconsult AS, Trondheim, Norway

List of Symbols

Δu	Increment in the radial displacement of the bolt tube during unfolding
Δs	Increment in the circumference of the bolt tube during unfolding
Δp	Increment in the water pressure during the unfolding of the bolt tube

Δd	Increment in the bolt diameter during unfolding
UCS	Uniaxial compressive strength
r	Average radius of the bolt tube during unfolding
q	Contact stress on the bolt–rock interface after installation
q_d	The contact stress in the diamond-drilled boreholes obtained by back-calculation
P	Ultimate pull load of the bolt
P_p	Ultimate pull load of the bolt in percussive boreholes
P_d	Ultimate pull load of the bolt in diamond-drilled boreholes
p_1	Maximum pressure applied on the borehole wall during bolt installation
L	Length of the expandable section of the bolt between the end bushings; $L = 360$ mm
l	Bond length of the bolt; $l = L - 2d_0$
K_r	Stiffness of the borehole in the rock mass
K_b	Average radial stiffness of the bolt tube
K_{bq}	Radial stiffnesses of the bolt tube during contraction after water pressure is removed
K_{bp}	Radial stiffnesses of the bolt tube during unfolding
F_s	Contact force on the tongue shoulder
F_c	Contact force on the side opposite the tongue
d_c	Diameter of the concrete core
d_b	Borehole diameter
d_0	The initial profile diameter of the bolt; $d_0 = 26.8$ mm
D	The fully unfolded diameter of the bolt; $D = 38.7$ mm
d	Bolt diameter during unfolding
φ_a	An additional friction angle expressing the asperities (or roughness) on the borehole wall
φ_b	The basic friction angle between the concrete and the bolt
α	The tilt angle at which the bolt section starts to slide on the concrete cores in tilt test
β	The angle between the lines from the center of the bolt to the centers of the two concrete cores in the cross section
λ	A coefficient representing the degree of recovery of the outward elastic displacement of the bolt tube during installation; $\lambda = 0$ when the outward elastic displacement is completely locked and $\lambda = 1$ when the outward elastic displacement completely recovers

1 Introduction

In most mining regions, ground support is a legislative requirement and is obligatory in most civil underground rock excavations. Rockbolting is the most widely used

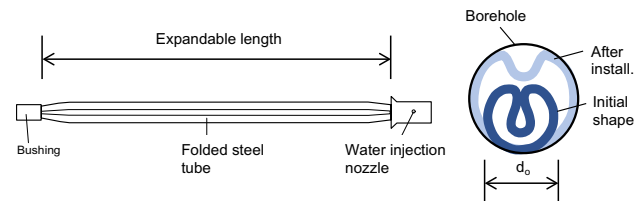


Fig. 1 Sketch illustrating the geometry of an inflatable rockbolt. Adapted from Li (2016)

underground support measure due to its excellent reinforcement capabilities and cost-effectiveness. Rockbolts can be classified into three types according to their anchoring mechanisms in the rock mass: discrete point (either two-point or multi-point) anchored bolts, fully grout bonded bolts, and friction bolts (Li 2017). These three types of rockbolts are used under different rock mass conditions and for different purposes, such as to provide temporary or permanent support. The rapid installation of ground support after excavation is vital to maintaining the integrity of the rock mass in abnormal geological conditions including water rushing, weakness zone and in cases where there is a risk of unravelling. In these cases, the use of inflatable bolts is a good choice to avoid uncontrollable collapses.

An inflatable bolt is made of a steel tube that is folded into an omega-shape in cross section (Fig. 1). These bolts are inserted into boreholes and expand as pressurized water is injected into the tube. Once the water pressure is removed the radial forces generated by the plastic deformation of the tube generate a radial compressive pressure applied to the surface of the borehole. The frictional resistance generated by this process anchors the rockbolt within the rock mass.

Swellex, the first inflatable rockbolt, was introduced in the 1980s (Wijk and Skogberg 1982). Several similar products have appeared in the market in the last twenty years since the patent of Swellex expired. These included the Omega bolt by DSI Underground (Turner and Green 2007), the EX300 by Sandvik (Bjurholt 2007), the X-Pandabolt by Epiroc (Epiroc 2022), the M3 Expandable Rock Bolt by Jenmar (Jenmar 2022), and the Expandable Rock Bolt by SSAB (SSAB 2022).

Previous studies have assessed the performance of inflatable bolts in both laboratory and field conditions (e.g., Wijk and Skogberg 1982; Grasselli 2005; Turner and Green 2007; Bjurholt 2007; Player et al. 2009; Li 2016; Scolari et al. 2017; Hagen et al. 2019). The reinforcement of rock mass by inflatable bolts was also analytically and numerically studied by Grasselli (2005) and Carranza-Torres (2009). However, there have only been a limited number of tests conducted on investigating influencing factors such as installation water pressure and borehole size (Håkansson and Li 1997; Soni 2000).

The behavior of inflatable bolts was first studied analytically by Wijk and Skogberg (1982) and later further developed by Håkansson and Li (1997), Li and Håkansson (1999), and Li (2016). Wijk and Skogberg (1982) assumed the rockbolt to be a circular ring after installation, which significantly deviates from the actual geometry of the bolt as it unfolds. When installed, the bolt is always partially unfolded, with the excess circumference bending inwards in a “tongue” shape. This tongue shape causes the radial stiffness of the bolt tube to be much smaller than the assumed circular ring; consequently, the friction at the surface of the bolt, and in turn, the load-bearing capacity of the bolt, is much lower than the estimates made by Wijk and Skogberg (1982). Li (2016) accounted for the influence of the tongue in his study and analytically investigated the effects of various parameters including the installation water pressure, borehole size and borehole roughness. Kim et al. (2017) numerically studied the influence of the bolt tongue on the distribution of contact stress along the perimeter of the inflatable bolt; their modeling results show that contact stress is not uniformly distributed along the perimeter of the bolt.

All analyses mentioned above stated that the pull load capacity of an inflatable bolt would increase with the borehole diameter or the unfolding degree of the bolt tube. However, field pull test results, for example by Soni (2000), showed that the pull load capacity of the bolt shattered in a large range following the change in the borehole diameter. The shattering could be caused by variations in the unfolding degree of the bolt and the borehole roughness. A series laboratory tests were conducted in the Rock Mechanics Laboratory of the Norwegian University of Science and Technology to clarify how the borehole diameter and roughness affect the pull load capacity of inflatable bolts.

This study aims to experimentally quantify the impact of borehole size, borehole roughness, and installation water pressure on the load-bearing capacity of inflatable bolts installed in a hard rock mass. Three borehole sizes, two types of boreholes (percussively and diamond-drilled, respectively) with different rough borehole surfaces, and two installation water pressures were examined in tests conducted in a laboratory setting.

2 A Brief of the Theoretical Analysis of the Inflatable Bolt

An inflatable rockbolt is anchored within a rock mass due to the friction between the bolt tube and the borehole wall. Its ultimate pull resistance P is expressed by:

$$P = \pi d_b l q \tan(\varphi_b + \varphi_a) \tag{1}$$

where d_b is the borehole diameter, l is the bond length of the bolt (i.e., the length in contact with the borehole), q is the contact stress on the bolt–rock interface, φ_b is the basic friction angle between the rock and the bolt, and φ_a is an additional friction angle expressing the asperities (or roughness) on the borehole wall.

Li (2016) proposed an analytical solution to the primary contact stress q between the bolt and the borehole wall by considering the elastic radial recoveries of the borehole and bolt tube deformations after bolt installation when the water pressure disappears. The primary contact stress is proportional to the maximum pressure p_1 applied to the borehole wall during bolt installation. The proportional coefficient between the two parameters is related to the radial stiffness of the rock mass (K_r), to the radial stiffnesses of the bolt tube during unfolding and contraction (K_{bp} and K_{bq} , respectively), and to the recovery degree of the outward elastic displacement of the bolt tube during installation (expressed by parameter λ). It should be noted that the stiffness parameters K_{bp} and K_{bq} are related to the bolt diameter. The primary contact stress q is expressed as (Li 2016):

$$q = \frac{K_{bq} K_{bp} - \lambda K_r}{K_{bp} K_{bq} + K_r} p_1 \tag{2}$$

The recovery parameter λ varies in the range of 0–1 with $\lambda = 0$ for zero recovery when the outward elastic displacement of the tube is completely locked in after installation, and $\lambda = 1$ for complete recovery when the elastic displacement rebounds completely and the bolt tube recovers to its non-stressing state. K_{bp} and K_{bq} are slightly different owing to the different loading conditions within the bolt tube during unfolding (with water pressure) and after the water pressure is removed. For the sake of simplicity, we assume that they are identical, such that $K_{bp} = K_{bq} = K_b$, where K_b represents the average radial stiffness of the steel tube. The above expression then becomes:

$$q = \frac{K_b - \lambda K_r}{K_b + K_r} p_1 \tag{3}$$

If the outward elastic radial displacement of the bolt tube during installation does not rebound at all, i.e., if $\lambda = 0$, and considering that $K_b \ll K_r$, the above expression becomes:

$$q \approx \frac{K_b}{K_r} p_1 \tag{4}$$

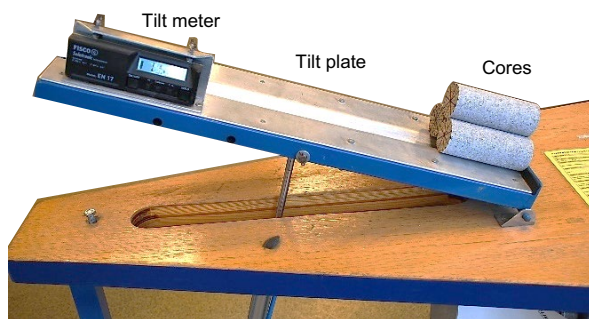
That means that, in the case where there is zero recovery in the outward elastic displacement of the bolt tube, the contact stress is approximately linearly correlated with the pressure applied to the borehole wall during installation. The

contact stress becomes zero when $(K_b - \lambda K_r) \leq 0$, or when the recovery coefficient is $\lambda \geq K_b/K_r$.

3 Auxiliary Tests

3.1 Tilt Tests

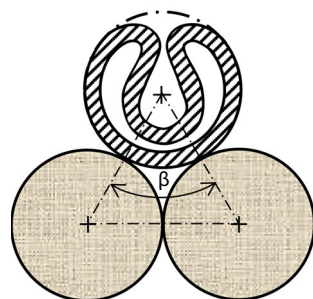
The ultimate pull load of an inflatable bolt installed in a rock mass is determined by the friction and the mechanical interlocking between the bolt and the borehole wall, which are expressed by the basic friction angle, φ_b , and the additional friction angle, φ_a , in Eq. 1, respectively. The basic friction angle between the bolt steel and the concrete host was measured using a tilt test (Fig. 2a). Cores were extracted from the concrete block within which the bolts were installed, and measurements were conducted using the three-core method (Alejano et al. 2018; Li et al. 2019), but with one of the cores replaced by a short section of the inflatable bolt. The two concrete cores were placed on the tilt plate of the apparatus with the axes of the cores oriented toward the tilt direction. The bolt section was placed on top of the two concrete cores (Fig. 2b).



(a)



(b)



(c)

Fig. 2 A schematic describing the tilt test used to determine the basic friction angle between the bolt steel and the concrete: **a** the tilt test apparatus, **b** the three-core measurement method, and **c** a sketch illustrating how angle β is determined from a cross-sectional plan of the cores

One end of the tilt plate is attached to the table using a hinge. During testing, the tilt plate is pushed upward by a pneumatic cylinder located in the middle of the plate (Fig. 2a). The free end of the plate is slowly and smoothly lifted upward, with the plate rotating around the hinge at the other end. The critical tilt angle is measured by a tilt meter that is fixed at the free end of the tilt plate. The bolt section begins to slide on the two concrete cores when the plate reaches a critical tilt angle α . The diameter of the concrete cores is $d_c = 26.61$ mm, and the initial profile diameter of the bolt section used in the test is $d_0 = 26.92$ mm. Figure 2c shows a schematic illustration of the cross section of the two concrete cores as well as the steel bolt tube. Let β represent the geometrical angle between the two center-to-center lines from the center of the upper steel tube to the two base concrete cores. The value of β was found to be 59.61° based on the diameters of the cores and the steel tube. The maximum friction angle between the bolt tube and the concrete cores can be calculated from the critical tilt angle α and the geometrical angle β according to Stimpson (1981). However, the experiments by Li et al. (2019) showed that the three-core method overestimated the friction angle for 2° compared to the method of using two-sawed rock pieces. Thus, the basic friction angle between the concrete and the bolt steel is calculated by subtracting the overestimated 2 degrees from the theoretical solution as follows:

$$\varphi_b = \arctan\left(\cos\frac{\beta}{2}\tan\alpha\right) - 2^\circ = \arctan(0.8676 \times \tan\alpha) - 2^\circ. \quad (5)$$

A total of 15 tests were conducted and the basic friction angle between the concrete and the bolt steel was found to be $\varphi_b = 13.97^\circ \pm 2.79^\circ$.

3.2 Uniaxial Compression Tests

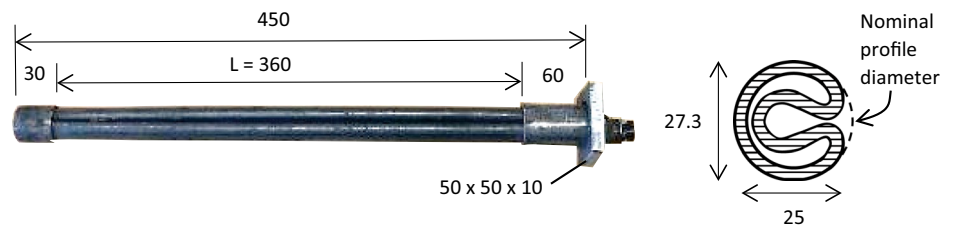
Uniaxial compression tests were conducted to determine the uniaxial compressive strength (UCS) and Young's modulus of the concrete block within which the inflatable bolts would be installed for the pull tests. Two cylindrical concrete samples were prepared from cores extracted from the concrete block. The specimens were 78.8 mm in diameter and 182.5 mm in length, corresponding to a length-to-diameter ratio of 2.3. The tests revealed that the concrete had an average UCS of 109 MPa and a Young's modulus 35.4 GPa. The concrete with such mechanical properties is equivalent to a hard rock block.

4 Bolt Specimens and Test Arrangements

4.1 Bolt Specimens

All tests used X-Pandabolt inflatable bolts that were provided by Epiroc (Fig. 3). The bolts are 450 mm long with an

Fig. 3 The inflatable X-Pan-dabolt used in the tests (all dimensions are measured in mm)



expandable middle section of 360 mm. The nominal initial profile diameter of the folded bolt is 27 mm, but the cross-section of the outer diameter is not perfectly circular with a maximum width of 27.5 mm and a minimum width of 25 mm in two orthogonal orientations as shown in Fig. 3. The nominal initial profile diameter refers to the maximum width of the folded bolt tube in the initial state. The nominal maximum diameter of the bolt tube after full unfolding is 38.5 mm, and the thickness of the bolt tube is 2 mm. The borehole size recommended by the bolt supplier is 32–36 mm, installed with a nominal water pressure ranging from 24 to 30 MPa (Epiroc 2022). The pump used in the tests is a High-Pressure Air pump provided by Epiroc with a maximum pressure of 30 MPa. Water is pumped into the bolt through a water injection nozzle on the bolt head during installation. The water injection nozzle is left open after installation, causing the water pressure in the tube to drop to zero.

4.2 Setup for the Unfolding of Bolts in Air

The contact stress between the bolt and the borehole wall is directly related to the radial stiffness of the unfolded bolt tube. The radial stiffness of the bolt is in turn related to the unfolding degree of the tube. The radial stiffness can be calculated on the unloading line of the installation water pressure versus the radial displacement of the tube that is unfolded in air.

A few inflatable bolts were unfolded in the air to examine the variation of the radial stiffness of the bolt during the unfolding of the bolt tube. Each bolt was fixed on a wood frame at the bolt ends, and a thin steel wire was wrapped around the bolt in the middle (Fig. 4). One end of the wire

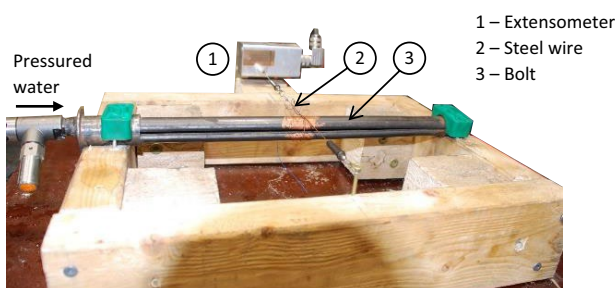


Fig. 4 The setup used to test the unfolding of the bolts in the air

was fixed to the wood frame while the other end was attached to an extensometer that was fixed to the opposite side of the frame, with the orientation of the wire perpendicular to the bolt axis. The extensometer measures the change in the circumference of the bolt, Δs , during unfolding under the water pressure. The increment in the bolt diameter, Δd , is expressed as $\Delta d = \Delta s / \pi$. The bolt diameter, d , can then be estimated as follows:

$$d = d_0 + \Delta s / \pi \tag{6}$$

where d_0 is the initial profile diameter of the bolt. While the nominal initial profile diameter of the bolts is 27 mm, the real bolt diameter varies slightly from bolt to bolt. Before each test, the initial profile diameter of each bolt was measured in three orientations in cross-section and at three locations along the length of the bolt. The average of the nine measurements was taken to be the initial profile diameter. It should be noted that the calculated bolt diameter d is an approximate estimation of the diameter of the equivalent circular bolt tube during unfolding. It is slightly underestimated because the measured increment in the circumference of the bolt, Δs , does not include the increment of the circumference facing the opening of the tongue (i.e. the section marked by the dash line in Fig. 3).

4.3 Pull Test Setup

The bolt samples were installed in a cubic concrete block with dimensions of 95 cm. The UCS of the concrete was 109 MPa (see Sect. 3.2). Each test involved pulling a bolt until a displacement of approximately 120 mm was observed. The following conditions were tested: in smooth and rough boreholes of three diameters, and under two installation water pressures (24 and 30 MPa). A total of 18 bolts were pull tested. The test conditions of each bolt are presented in Table 1.

Rough boreholes were drilled using a pneumatical percussive drill rig (Fig. 5a). Smooth boreholes were drilled using a diamond drill rig (Fig. 5b). The cores from the diamond drilling were used for the tilt tests.

Different hole diameters were used to examine the influence of the degree of unfolding of the bolt tube on the pull load capacity. The percussively drilled holes were, on

Table 1 The number of bolts used for each of the testing conditions investigated in this study

Number of bolts	Hole diam. (mm)	Drill method	Borehole condition	Water pressure (MPa)
4	37	Percussive	Rough	30
4	36	Diamond	Smooth	30
2	37	Percussive	Rough	25
2	33.5	Percussive	Rough	30
2	33	Diamond	Smooth	30
2	31	Percussive	Rough	30
2	30	Diamond	Smooth	30

average, 0.5–1 mm larger than the diameters of the drill bits, but the diamond-drilled holes were relatively smooth and their diameters were generally identical to the drill bit diameters. The differences in roughness in the percussive and diamond-drilled holes can be seen in the photographs presented in Fig. 6.

Sixteen (16) of the 18 bolts were installed with a nominal water pressure of 30 MPa, with the remaining two installed at a water pressure of 24 MPa. There were slight deviations in installation water pressure compared to the nominal values. Once the water pressure reached the nominal installation values, the pressure was held for 60–80 s to ensure the rockbolt conformed to the perimeter of the borehole.

Fig. 5 Images showing how **a** the percussive and **b** diamond-drilled boreholes were drilled in the concrete block

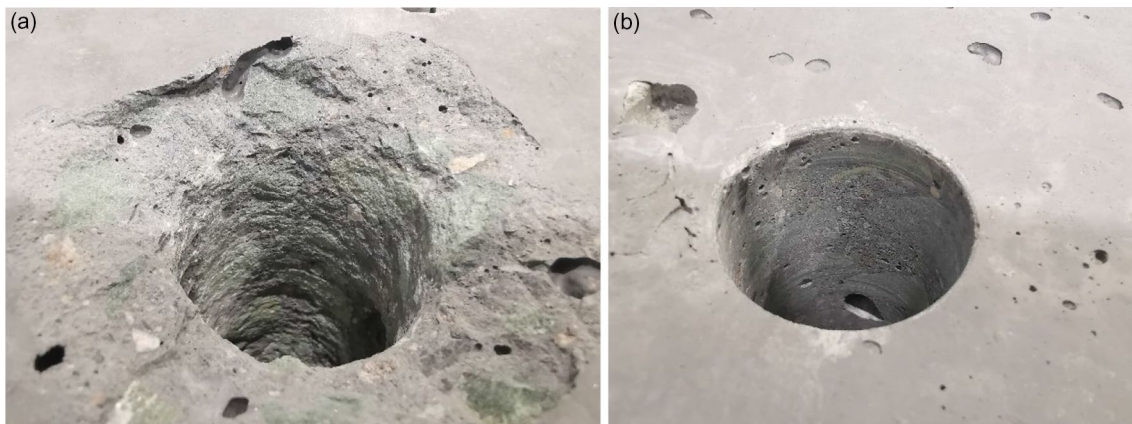
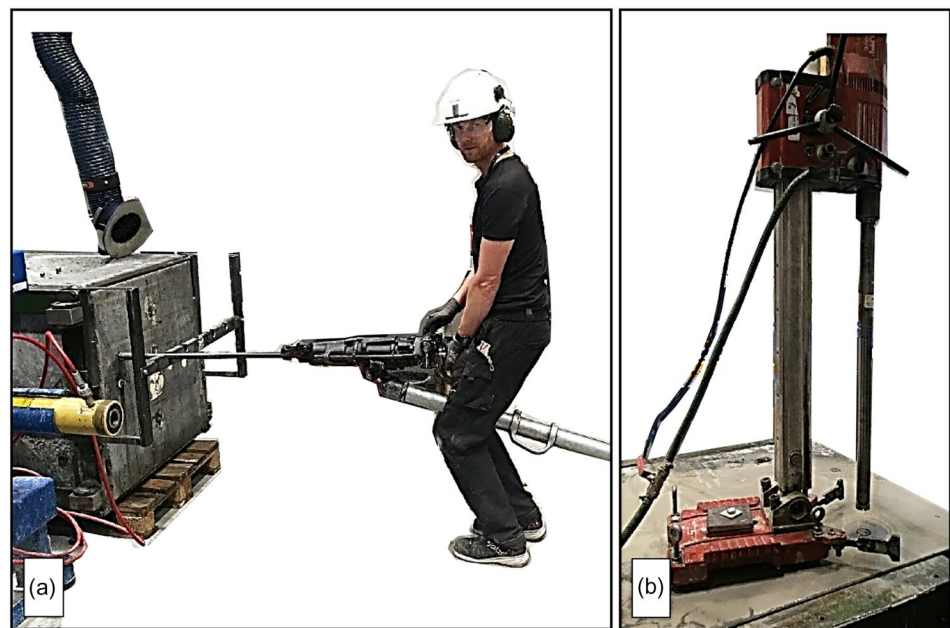


Fig. 6 Images showing the roughness of **a** a percussive borehole and **b** a diamond-drilled borehole

The boreholes were spaced 150 mm apart from each other and from the edges of the concrete block. This spacing limits the influence of each hole on neighboring boreholes. Figure 7a shows the layout of the 16 holes drilled on a single side of the block. Additional holes were drilled on another side of the block. Figure 7b shows an example of some bolts that have already been installed within the block.

4.4 Pull Test Procedure

A clevis with a drawbar was used to apply a load using a hydraulic cylinder during pull testing (Fig. 8a). The testing apparatus and the measurement instruments are shown in Fig. 8b. The displacement of the bolt was measured using an extensometer (A) attached to the upper end of the connecting rod. The elastic deformation of the connecting rod

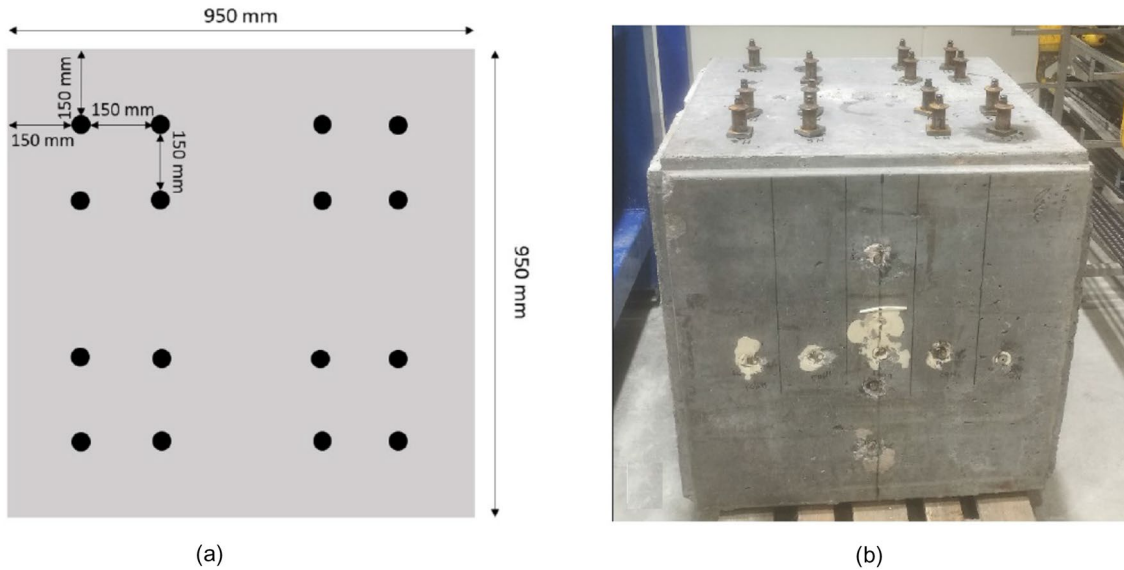
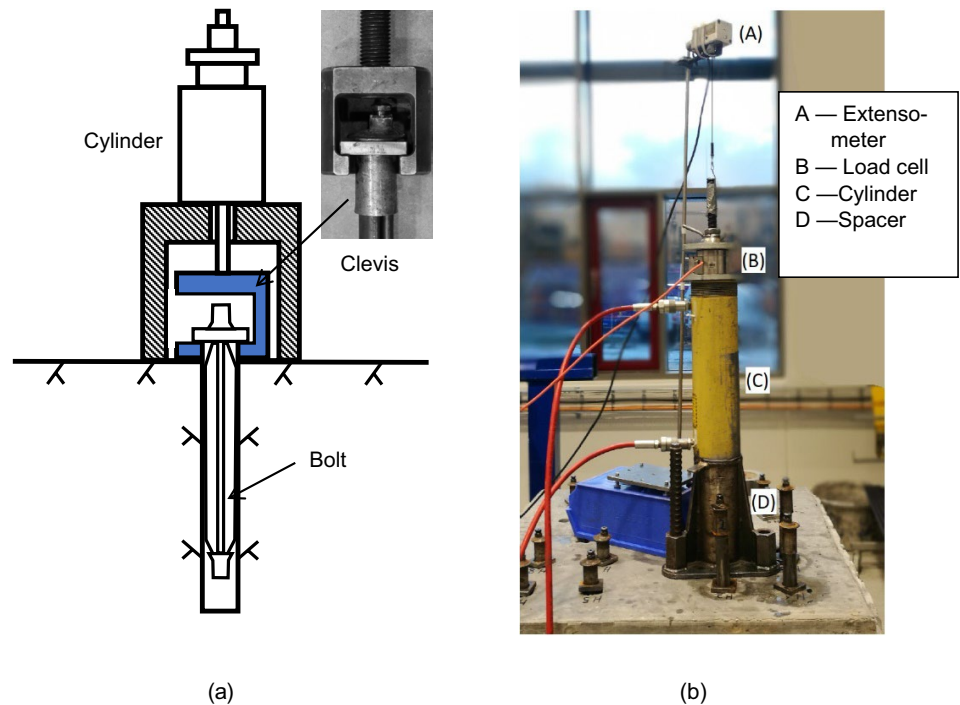


Fig. 7 a Layout of the drilled holes on a single side of the concrete block. b Image showing an example of some installed bolts

Fig. 8 The testing setup: a a sketch illustrating the testing configuration, and b an image of the testing apparatus



is negligible; therefore, the displacement observed was assumed to be the displacement of the bolt. The load cell (B) was placed between the head plate and the ram of the cylinder.

The cylinder was driven by the oil pressure of an electrical pump. The pull load was applied at a speed of approximately 1 kN/s, which takes approximately 1–2 min to reach the maximum load. For most of the bolt samples, the test was terminated after approximately 120 mm displacement. Typically, the pull tests were conducted 5–7 days after installation, but one group (no. 15–18) was tested 3 weeks after installation because of the delay in the availability of the test setup. It is believed that the delay would not affect the test results taking into account that the contact stress between the bolt and the concrete would not change in such a short period.

5 Testing and Test Results

5.1 Unfolding of the Bolt in the Air

A total of eight bolts were unfolded in the air, with four of them loaded in cycles. Loading cycles were conducted for every bolt sample to determine the radial stiffness of the bolt tube in different unfolding degrees. Figure 9 shows a plot of the water pressure versus the diameter of bolt B36 (one of the bolts tested in loading cycles). The curves of the other three bolts in the group were found to be relatively similar and are presented in Figs. 24, 25 and 26 in the Appendix. The diameter of the bolts during unfolding was measured by the method introduced in Sect. 4.2. Loading cycles were conducted to determine the radial stiffness of the bolt at different degrees of unfolding. Photographs of the degrees of

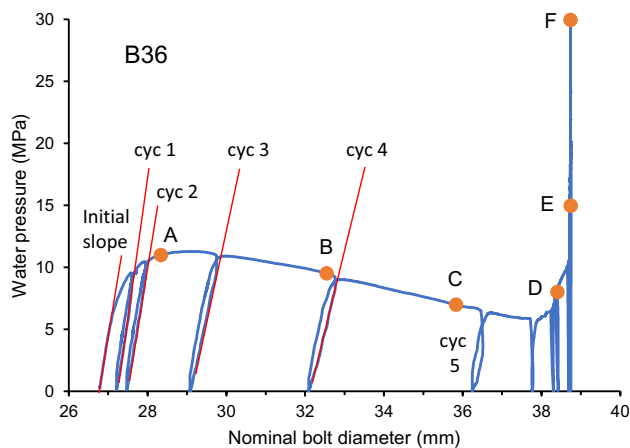


Fig. 9 Water pressure plotted against the bolt diameter during the unfolding of bolt B36 in air. Water pressure (MPa)/bolt diameter (mm) at the marked points: A—11/28.33; B—9.5/32.54; C—7/35.83; D—8/38.4; E—15/38.74; F—30/38.74

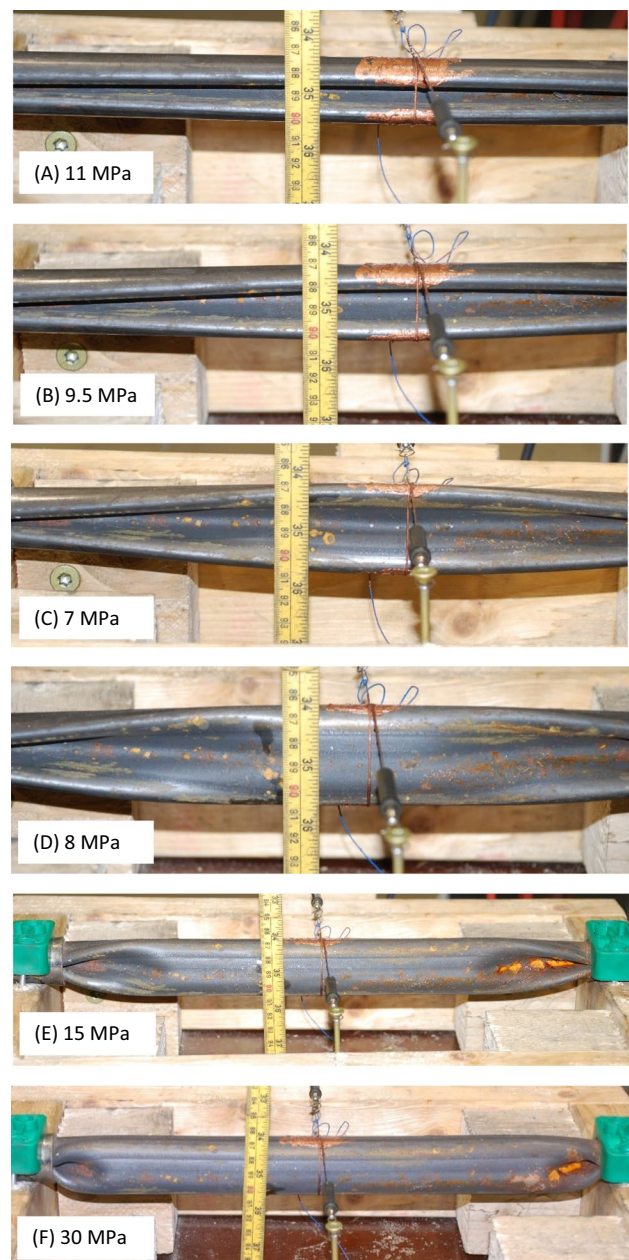
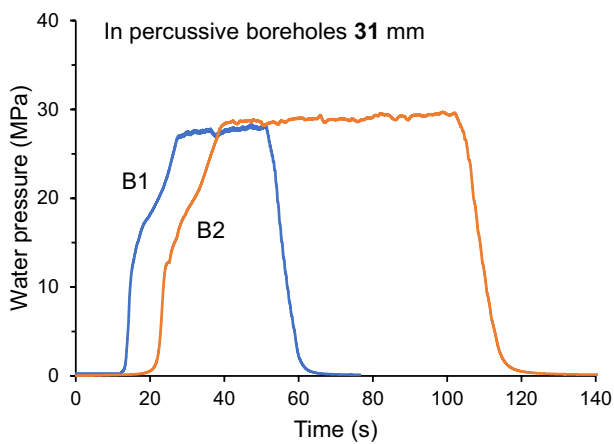


Fig. 10 Images of bolt B36 as it unfolded at each of the six moments corresponding to points A, B, C, D, E, and F in Fig. 9. The water pressure at each moment is also included in the image

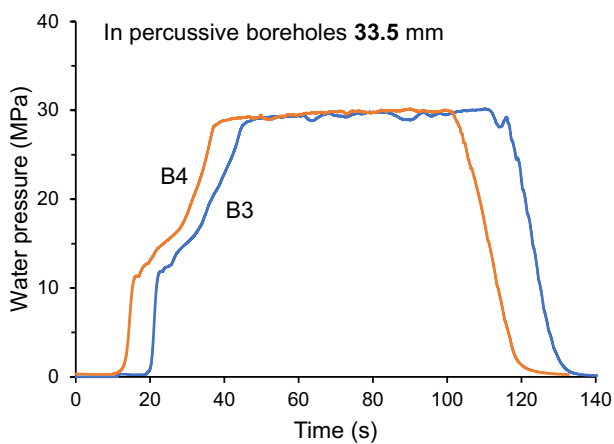
unfolding at points A, B, C, D, E and F on the pressure–diameter curve of bolt B36 (Fig. 9) can be found in Fig. 10.

5.2 Water Pressure During Bolt Installation

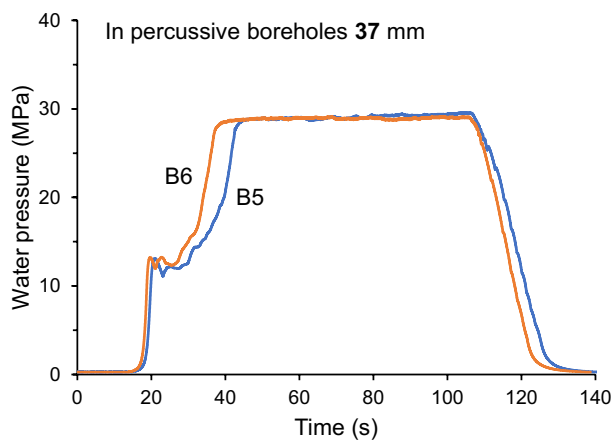
The variation in the water pressure during bolt installation is presented in Fig. 11. The figures also show the difference in behavior caused by the different borehole diameters. All six bolts presented were installed with a water pressure of 30 MPa.



(a)



(b)



(c)

Fig. 11 Variations of the water pressure over time for bolts installed in percussively drilled boreholes with a water pressure of 30 MPa: **a** bolts B1 and B2, **b** bolts B3 and B4, and **c** bolts B5 and B6

In the 31-mm boreholes (Fig. 11a), the bolt tube yielded at around 12 MPa, indicating that the tube started to plastically expand. After that, the water pressure continued to increase monotonically until the pressure reached a level close to 30 MPa at 18–20 s at which the bolt tube had been unfolded to the diameter of the borehole and the exterior surface of the bolt was tightly compressed against the borehole wall. The water pressure then remained approximately constant at this level until pumping was terminated.

In the 33.5-mm boreholes (Fig. 11b), the variation in the water pressure was similar to that observed in the 31-mm boreholes, but the rate of increase in water pressure was lower after the water reached its yield pressure at around 12 MPa. The bolts were unfolded to the diameter of the boreholes at around 25 s.

In the 37-mm boreholes (Fig. 13), the bolt tube yielded at around 12.5 MPa, then the water pressure dropped to a slightly lower level for a short period before increasing again until the bolt tubes were unfolded to the diameter of the boreholes at 25–28 s. The pressure drop after the yield point is superficially similar to the pressure curves observed in bolts unfolded in the air (Fig. 9).

5.3 Pull Test Results

The testing conditions and ultimate pull load for each bolt are presented in Table 2. The pull tests were carried out

Table 2 Borehole diameters, installation parameters, and ultimate pull loads of all bolt samples

Bolt no	Hole diam. (mm)	Drill method	Installation water pressure (MPa)	Ultimate pull load (kN)
B1	31	Percussive	30/28*	60.24
B2	31	Percussive	30	75.01
B3	33.5	Percussive	30	46.61
B4	33.5	Percussive	30	44.80
B5	37	Percussive	30	84.33
B6	37	Percussive	30/29*	78.68
B7	37	Percussive	24/25*	63.49
B8	37	Percussive	24/25*	62.07
B9	36	Diamond	30/29*	57.98
B10	36	Diamond	30/29*	44.38
B11	33	Diamond	30	28.61
B12	33	Diamond	30	35.47
B13	30	Diamond	30	47.82
B14	30	Diamond	30	37.43
B15	37	Percussive	30	78.37
B16	37	Percussive	30	73.67
B17	36	Diamond	30	39.58
B18	36	Diamond	30	37.32

* The preset pressure/the measured pressure

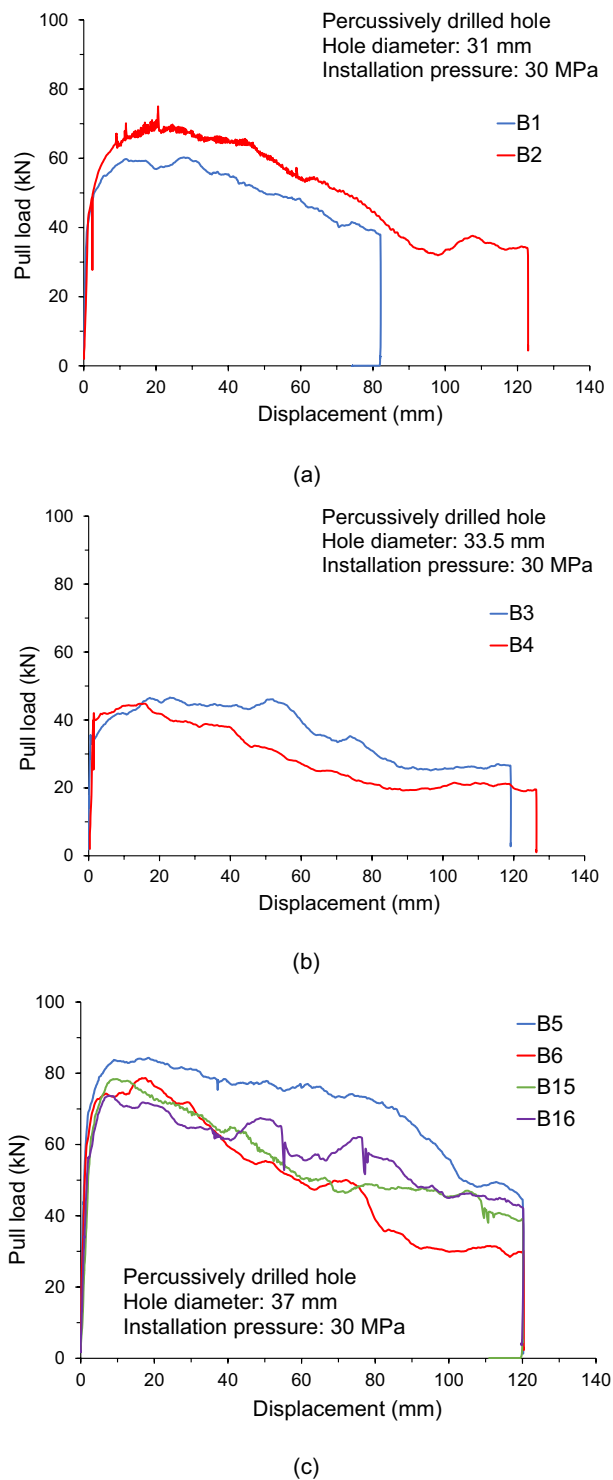


Fig. 12 The curves of ultimate pull load against displacement for bolts installed in percussively drilled boreholes with a water pressure of 30 MPa: **a** bolts B1 and B2 in 31-mm boreholes, **b** bolts B3 and B4 in 33.5-mm boreholes, and **c** bolts B5, B6, B15, and B16 in 37-mm boreholes

5–7 days after installation for bolts B1–B14 and 21 days after installation for B16–B18.

The curves of the pull load against bolt displacement for the bolts installed with a water pressure of 30 MPa in percussively drilled boreholes of 31 mm, 33.5 mm, and 37 mm are presented in Fig. 12a, b, and c, respectively. Figure 13 shows the curves of the bolts installed in 37-mm boreholes with a water pressure of 24 MPa.

The curves of the pull load against bolt displacement for the bolts installed with a water pressure of 30 MPa in diamond-drilled boreholes of 30 mm, 33 mm, and 36 mm are presented in Fig. 14a, b and c, respectively.

The load–displacement curves of all bolts tested under identical conditions are relatively consistent with deviations of approximately 10 kN observed in the ultimate pull load, with the exception of one bolt (B9) installed in a 36-mm diamond-drilled borehole (Fig. 14c). The ultimate pull load of bolt B9 is noticeably higher than the other bolts within the group, with a deviation of around 25 kN compared to the bolt with the lowest ultimate pull load.

6 Analysis of the Test Results

6.1 Radial Stiffness of the Bolt Tube During Unfolding

The contact stress between the bolt and the borehole wall is approximately linearly correlated to the radial stiffness of the bolt tube, as described by Eq. 4. Li (2016) provided his theoretical solutions to the relationship by considering the change in the geometry of the bolt during unfolding, but it is difficult to analytically calculate this change. The experimental data of the unfolding tests in the air can be used to determine the approximate radial stiffness of the bolt tube. It should be noted that this is only an approximate radial stiffness because the shape of the unfolding tube in the air is never completely circular, and the nominal diameter is instead calculated from the change in the circumference of the unfolding tube.

The red straight lines in Fig. 9 are the tangential lines to the initial linear segment of the pressure–diameter curve and to the linear unloading lines of the first three loading cycles for bolt sample B36. The slope of each line represents the radial stiffness of the bolt tube at that specific unfolding degree. Theoretically, the radial stiffness of a thin circular tube is defined by:

$$K_b = \frac{\Delta p}{\Delta u} r \quad (7)$$

where r is the average radius of the tube during unfolding, Δu is the increment in the radial displacement of the tube,

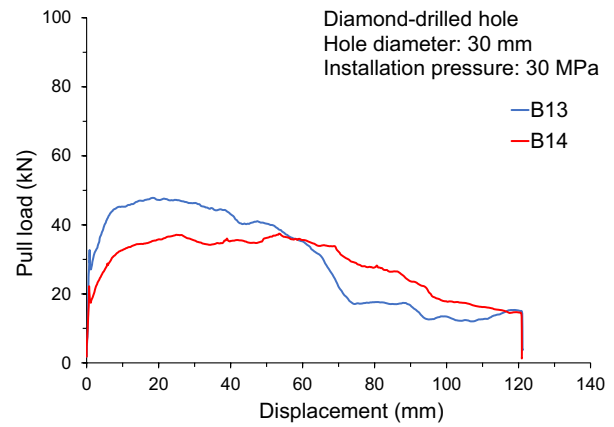
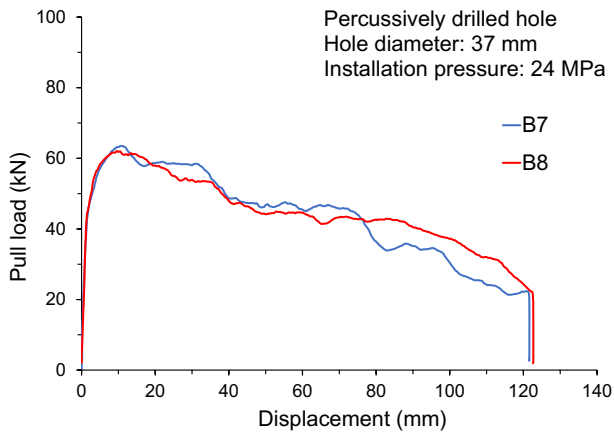


Fig. 13 The curves of ultimate pull load against displacement for bolts B7 and B8 in the 37-mm percussively drilled boreholes. These bolts were installed with a water pressure of 24 MPa

and Δp is an increment in the water pressure within the tube. The radial stiffnesses of bolt B36 at the start of loading and at each of the designated points during the first five loading cycles are calculated according to Eq. 7; these results are presented in Fig. 15. The unloading lines of all loading cycles after the fifth cycle were not linear, and do not truly reflect the stiffness of the bolt tube due to the frictional hysteresis of the measurement wire as well as the extremely small recovery deformations of the almost fully unfolded tube after unloading.

Figure 15 shows that the radial stiffness of the bolt in the first two loading cycles only deviated slightly from its initial stiffness of 532 MPa. The initial profile diameter of the bolt was 26.8 mm. In cycles 1 and 2, the tube diameter slightly increased to 27.2 mm and 27.5 mm, respectively. The third cycle was conducted immediately after the water pressure passed its peak value of approximately 12 MPa when the bolt tube was unfolded to a diameter of 29.1 mm. The radial stiffness dropped noticeably by approximately 20% to 412 MPa in the third cycle. The stiffness dropped even further to 377 MPa in the fourth cycle as the bolt diameter was increased to 32.1 mm. However, the stiffness rose to 550 MPa in the fifth cycle as the bolt diameter unfolded to 36.2 mm. The radial stiffness of the bolt could not be calculated in any cycles following this because of the reasons described above, but theoretically, the stiffness should quickly increase such that it approaches the stiffness observed when the tube reaches its fully unfolded diameter. Let us define the degree of unfolding of the bolt by the ratio of the increment in the nominal diameter to the difference between the fully unfolded diameter and the initial profile diameter of the bolt:

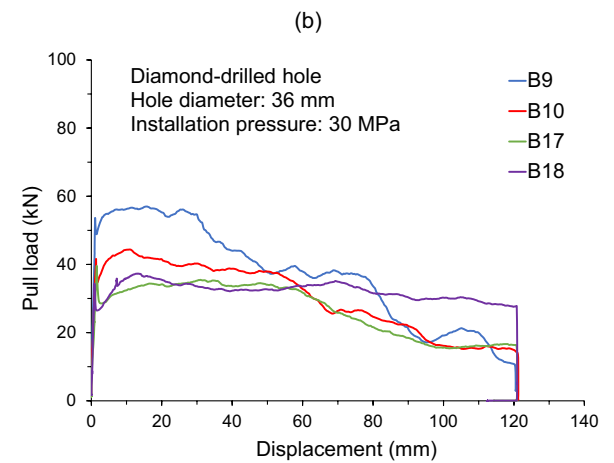
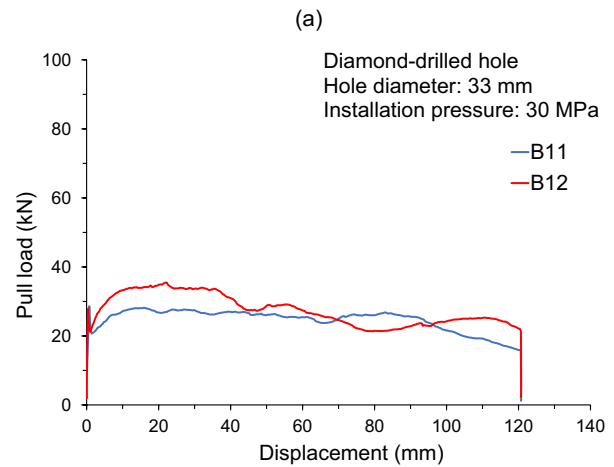


Fig. 14 The curves of ultimate pull load against displacement for bolts installed in diamond-drilled boreholes with a water pressure of 30 MPa: **a** bolts B13 and B14 in 30-mm boreholes, **b** bolts B11 and B12 in 33-mm boreholes, **c** bolts B9, B10, B17, and B18 in 36-mm boreholes

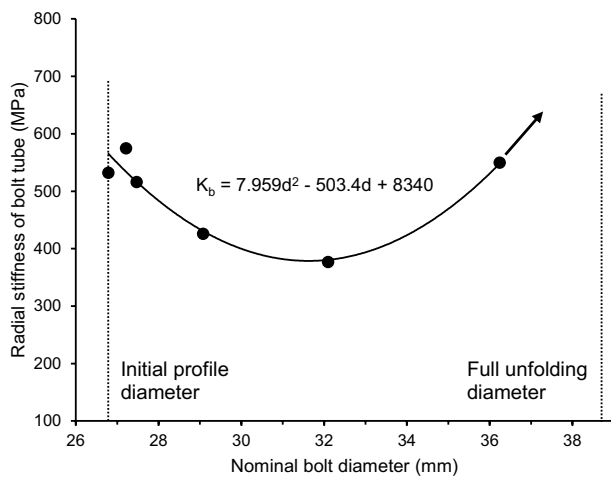


Fig. 15 The radial stiffness of bolt B36 against the nominal diameter of the bolt during unfolding in the air

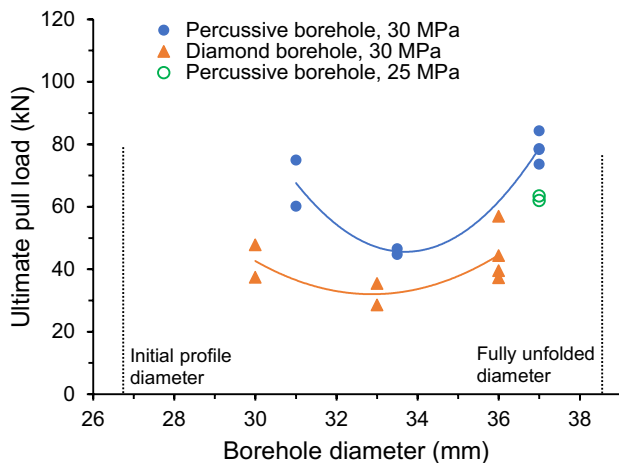


Fig. 16 The curve of the ultimate pull load against the borehole diameter for all tested bolts

$$\omega = \frac{d - d_0}{D - d_0} \quad (8)$$

where ω represents the degree of unfolding such that $\omega = 0$ in its initial state (i.e., without any unfolding) and $\omega = 1$ at the fully unfolded state; d_0 is the initial profile diameter of the bolt; d is the current nominal diameter; and D is the fully unfolded diameter of the bolt. The bolt exhibits its lowest radial stiffness in boreholes between 30 and 34 mm, corresponding to a degree of unfolding of 0.3–0.6.

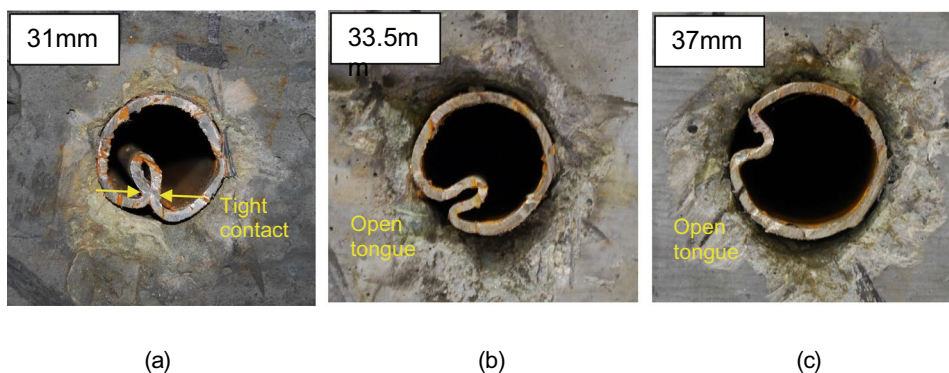
6.2 Impact of Borehole Diameter on Ultimate Pull Load Capacity

The ultimate pull loads of the tested bolts presented in Table 2 are plotted against borehole diameter in Fig. 16. The data in the figure are presented in three groups: one group for the bolts in percussive boreholes installed using a water pressure of 30 MPa, one group for the bolts in diamond drilled boreholes installed using a water pressure of 30 MPa, and one group for the two bolts in the 37-mm percussive boreholes installed using a water pressure of 24 / 25 MPa (the nominal value / the measured value).

For both percussive and diamond-drilled boreholes, the ultimate pull load is relatively high in the smallest boreholes (31 and 30 mm), lowest in the middle-sized holes (33.5 and 33 mm), and rises again in the largest boreholes (36 and 37 mm). This variation suggests that the contact stress on the borehole wall is lowest in the middle-sized boreholes. This trend is consistent with the variation in the radial stiffness of the bolt with borehole diameter as shown in Fig. 15, but not at the same borehole diameters. The radial stiffness of the bolt is close to its minimum when the bolt is unfolded to a diameter of 31 mm; theoretically, both the contact stress and the ultimate pull load should thus also be close to a minimum in a 31-mm borehole. However, the ultimate pull loads of the two bolts in the 31-mm percussive boreholes are quite high (Fig. 16). This suggests that there must be a missing factor in our calculation of the contact stress in Eq. 4.

The bolts were cross-sectionally cut after the tests. The images in Fig. 17 show the cross sections of three bolts installed in 31-mm, 33.5-mm, and 37-mm percussive boreholes. The degrees of unfolding in the three boreholes are 0.35, 0.56, and 0.86, respectively, as calculated by Eq. 8. It was observed that the shape of the bolt tongue (i.e., the folded portion of the tube) was different in each of the three differently sized boreholes. In the smallest borehole (31 mm; Fig. 17a), the shoulders of the tongue are tightly compressed each other, indicating that the bolt tube could not contract radially after the removal of the installation water pressure, as assumed in the theoretical calculations. Therefore, the elastic deformation of the bolt tube was partially locked, resulting in additional contact stress between the bolt and the borehole. This resulted in a high ultimate pull load in the small borehole. In this case, Eq. 4 cannot be used to estimate the contact stress between the bolt and the rock. The shoulders of the bolt tongue were not in contact with each other in the 33.5-mm (Fig. 17b) and 37-mm (Fig. 17c) boreholes, which matches the geometry assumed in the theoretical calculations. The tongue was found to be shorter in the 37-mm borehole compared to the 33.5-mm borehole. The radial stiffness of the bolt, and consequently the contact stress and the ultimate pull load, are therefore higher in the

Fig. 17 The geometry of the unfolded inflatable bolts in percussive boreholes of **a** 31 mm (bolt B1), **b** 33.5 mm (bolt B4), and **c** 37 mm (bolt B5)



larger 37-mm borehole. This is consistent with the theory described by Eqs. 4 and 1.

6.3 Impact of Borehole Roughness on Ultimate Pull Load Capacity

Figure 16 shows that the curve of the ultimate pull load for the bolts installed in percussive boreholes is higher than the curve for the bolts installed in diamond-drilled boreholes, which shows that borehole roughness plays a role in enhancing the pull load capacity of the inflatable bolt. The diamond-drilled boreholes are very smooth, and thus the pullout resistance is determined almost exclusively by the friction between the bolt steel and the concrete material. The difference between the two fitting curves is representative of the contribution of the roughness of the percussive borehole to the pull load capacity of the bolts. The basic friction angle of the bolt-concrete contact is $\varphi_b = 14.97^\circ$ (Sect. 3.1). The contact stress on the borehole wall can be obtained using Eq. 1 by assuming that the additional friction angle $\varphi_a = 0$ in the diamond-drilled boreholes. The contact stress should be identical in percussive and diamond-drilled boreholes of the same diameter.

A short section of the bolt tube at either end of the bolt sample could not be unfolded to the borehole diameter due to the constraints enforced by the end bushings. It was observed after full unfolding of the bolt tube that this transition zone was approximately equal to the initial profile diameter d_0 of the bolt. Assuming that the length of the transition zone is equal to d_0 , the bond length of the bolt becomes $l = (L - 2d_0)$ where L is the length of the bolt between the end bushings (360 mm). Thus, the contact stress can be calculated as follows:

$$q_d = \frac{P_d}{\pi d(L - 2d_0)\tan\varphi_b} \tag{9}$$

where q_d is the contact stress in the diamond-drilled boreholes obtained by back calculations, and P_d is the ultimate pull load of the bolt in the diamond-drilled borehole. The contact stresses in the three differently sized diamond-drilled

boreholes were calculated according to Eq. 9 and presented in Fig. 18. The contact stress is lowest in the middle-sized 33-mm borehole compared to the 30-mm and 36-mm boreholes.

The additional friction angle φ_a of all percussive boreholes should be similar since they were drilled using the same pneumatic drill rig, though the drill bits may cause negligible deviations among the holes. The additional friction angle of the boreholes can thus be calculated using Eq. 1 from the contact stress obtained from Eq. 9. The additional friction angle is calculated as follows:

$$\varphi_a = \text{atan} \left[\frac{P_p}{\pi d q_d (L - 2d_0)} \right] - \varphi_b \tag{10}$$

where P_p is the ultimate pull load of the bolt in the percussive borehole. The shoulders of the tube tongue in bolts installed in the small 30-mm (diamond-drilled) and 31-mm (percussively drilled) boreholes were found to be in close contact as shown in Fig. 17a. In these cases, the contact stress in the small boreholes is related to both the borehole diameter and the locking of the tongue shoulder. In the boreholes of 33.5 and 37 mm, the tongue shoulders of the bolts were open, as shown in Fig. 17b and c; hence, the contact

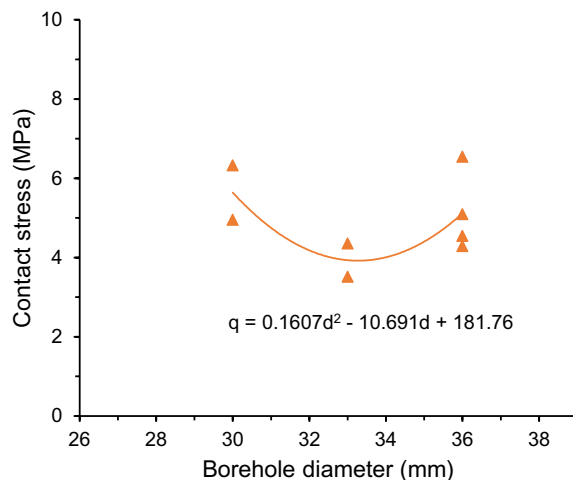


Fig. 18 The calculated contact stress of the bolts installed in diamond-drilled boreholes

Table 3 Estimated additional friction angles of the 33.5-mm and 37-mm percussively drilled boreholes

Bolt no	Hole diam. (mm)	Ultimate pull load (kN)	Contact stress ^a (MPa)	Additional friction angle ϕ_a ^b (°)
B3	33.5	46.61	3.96	5.94
B4	33.5	44.80	3.96	5.19
B5	37	84.34	6.19	7.31
B6	37	78.68	6.19	5.95
B15	37	78.37	6.19	5.88
B16	37	73.67	6.19	4.72
			Mean	5.83
			SD	0.88

^aCalculated using the regression equation $q=0.1607d^2-10.691d+181.76$

^bCalculated according to Eq. 10

stress is likely to be solely related to the borehole diameter regardless of whether the borehole was drilled using a diamond or percussive drill. It is assumed that the contact stress in diamond-drilled holes is identical to the percussively drilled holes. The contact stresses in the 33.5-mm and 37-mm percussive boreholes were calculated using a regression equation in Fig. 18, and the additional friction angles of the percussive boreholes were estimated using Eq. 10. The results of these calculations are presented in Table 3. The mean additional friction angle was found to be 5.83° with a standard deviation of 0.88° .

6.4 Impact of Installation Water Pressure on Ultimate Pull Load Capacity

Four bolt samples (B6, B7, B15, and B16) were installed with a water pressure of 30 MPa and two bolt samples (B7 and B8) were installed with a water pressure of 24 MPa in the 37-mm percussive boreholes. The ultimate pull loads of

bolts installed with the same water pressure were spread over a narrow range (Table 2, Fig. 16). The average ultimate pull load was 78.8 kN for bolts installed at 30 MPa water pressure and 62.8 kN for bolts installed at 24 MPa. It suggests that the ultimate pull load of the bolts decreases as the installation water pressure decreases. More investigation is required before any confident conclusion can be made about this trend, as only two water pressures were used in the tests.

6.5 Contact Area Between the Bolt and the Borehole Wall

The scratch marks on the exterior surface of the bolt tubes after pullout demonstrated that contact between the borehole and the bolt was not achieved along the entire perimeter. Figure 19 shows the scratch marks on the surface of bolt B2, which was installed in a 31-mm percussive hole. Based on the positions of the scratch marks, the bolt contacted the borehole walls in three locations on the exterior perimeter of the bolt: the two shoulders and the area on the opposite side of the tongue. Conversely, the bolt did not make contact with the borehole wall in three zones: the tongue opening, and in the areas approximately 90° and 270° from the center of the tongue opening. Due to the presence of the tongue, approximately 10–20 mm of the bolt profile did not make contact with the wall of a 31-mm borehole.

Figure 20 shows the scratch marks on the surface of bolt B7, which was installed in a larger 37-mm percussive hole. The scratch marks on this bolt are distributed slightly differently from those on the bolts installed in 31-mm boreholes. The scratches were still found in the same three locations as the smaller borehole, i.e., the tongue shoulders and the area opposite the tongue, but the total area of the profile in which no contact was achieved made up a larger percentage of the total perimeter. This means that the contact between the bolt and the borehole was narrower in the 37-mm borehole compared to the 31-mm borehole.

Fig. 19 Scratch marks on the exterior surface of bolt B2 after pullout testing. This bolt was installed in a 31-mm percussively drilled borehole. The contact zones are marked with red lines around the bolt tube

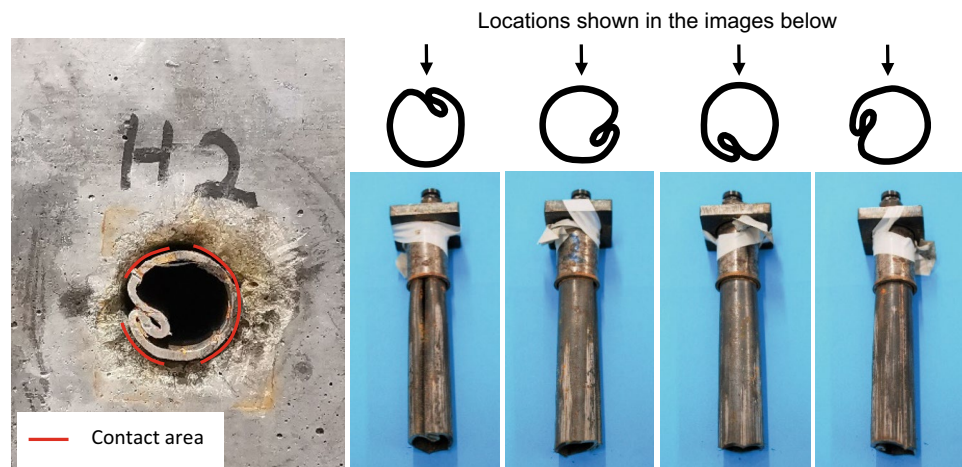


Fig. 20 Scratch marks on the exterior surface of bolt B7 after pullout testing. This bolt was installed in a 37-mm percussively drilled borehole

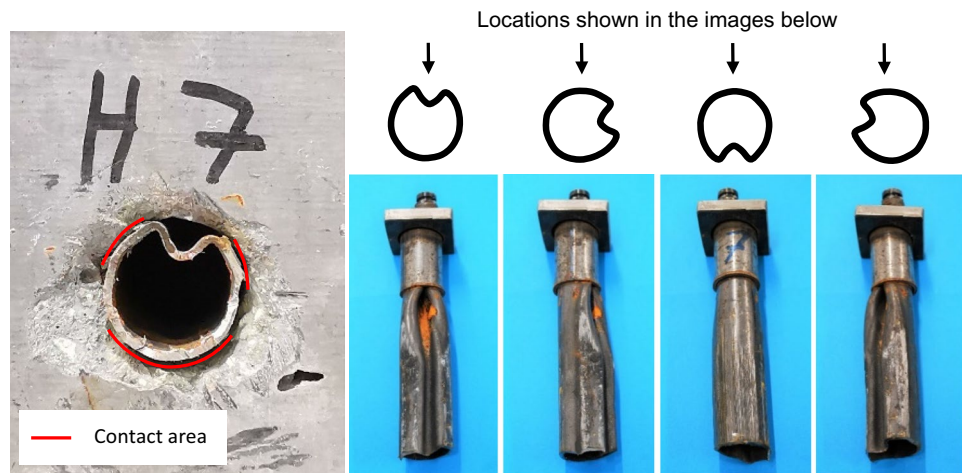


Fig. 21 Scratch marks on the exterior surface of bolt B8 after pullout testing. This bolt was installed in a 36-mm diamond-drilled borehole

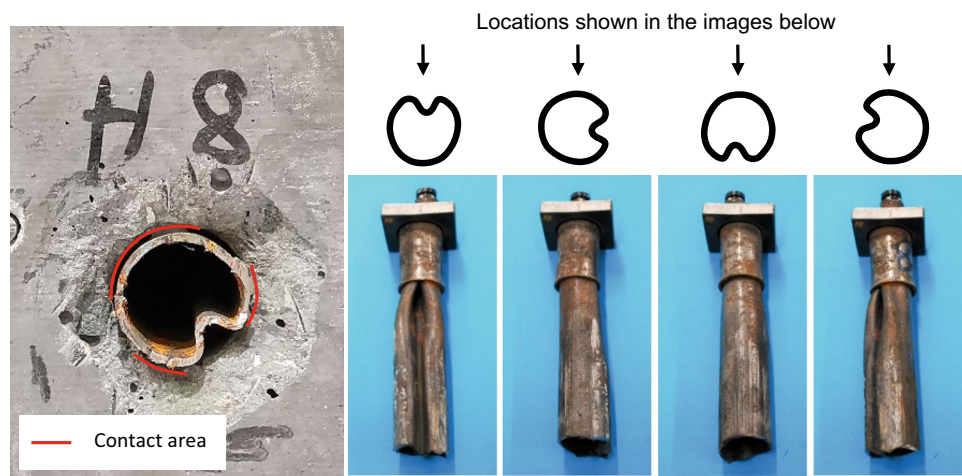


Figure 21 shows the scratch marks on the surface of bolt B8, which was installed in a diamond-drilled 36-mm borehole. Compared to the percussive borehole in which bolt B7 was installed, the B8 borehole diameter was only slightly smaller while the surface of the borehole walls was much smoother. The distribution of the scratch marks on bolt B8 was similar to bolt B7, suggesting that the contact profiles were relatively similar.

The comparison between the distribution of the scratch marks on the three bolts that were installed in boreholes of different sizes (31 and 37 mm) and different surface roughness (percussive and diamond-drilled) shows that the contact area is larger in smaller boreholes but is independent of borehole roughness.

Numerical modeling conducted by Kim et al. (2017) identified three contact zones in the half of the bolt perimeter ranging from 0° to 180° counting from the center of the tongue opening as shown in Fig. 22. The first zone ranging in 30°–50° and the third zone ranging in 115°–180°, were consistent with the observations made

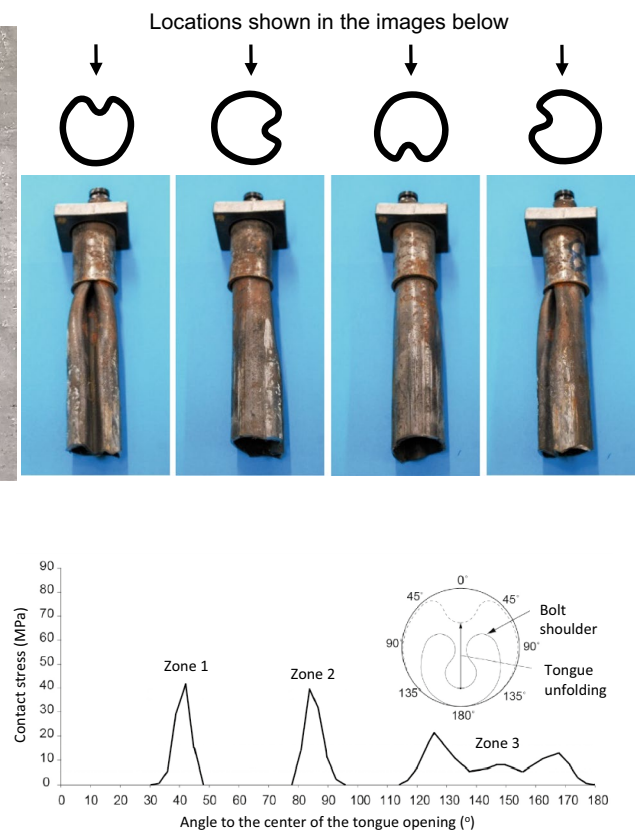


Fig. 22 The distribution of contact stresses along the perimeter of the inflatable bolt tube according to numerical modeling (Kim et al. 2017)

in this study; however, the second contact zone (80°–90°) was not observed in any of the bolt samples.

The analyses above suggest that the inflatable bolt is anchored within the borehole by three radial forces: two symmetrical forces on the tongue shoulders ($2 \times F_s$) and one on the

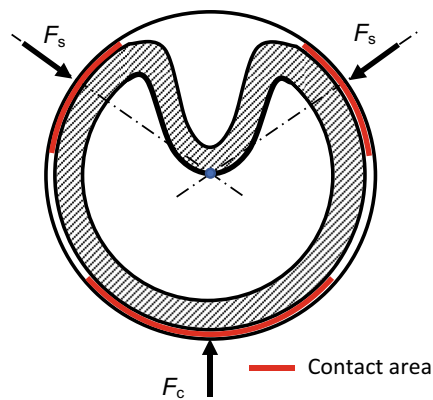


Fig. 23 A simplified sketch illustrating the contact forces between the inflatable rockbolt and the borehole wall in cross-section

opposite side of the tongue (F_c), as shown in Fig. 23. The contact lengths in the three locations vary with borehole diameter, with the largest contact areas observed in smaller boreholes.

7 Conclusion

A series of pullout tests were conducted on inflatable rockbolts under laboratory conditions. The tests aimed to quantify the influence of borehole size, borehole roughness, and installation water pressure on the ultimate pull load capacity of the bolt. The following conclusions were drawn from the test results.

The radial stiffness of the bolt tube is lowest in the middle-sized borehole and increases in both larger and smaller boreholes. The radial stiffness of the bolt directly affects the contact stress and thus the frictional pull resistance of the bolt.

The pull load capacity of the inflatable bolt is minimum when the borehole diameter is in the middle of the initial profile diameter and the fully unfolded diameter of the bolt tube. The pull load capacity increases as the size of the borehole becomes larger or smaller. In small boreholes, the two shoulders of the tube tongue are clamped, which prohibits the recovery of the outward elastic deformation of the bolt tube and thus results in higher contact stress and consequently higher pull load capacities. In the middle-sized and larger boreholes, the pull load capacity is dominantly dependent on the radial stiffness of the bolt. Therefore, the pull load capacity starts to increase with an increase in the borehole diameter from the middle-size borehole.

The test results demonstrated that borehole roughness is vital in enhancing the pull load capacity of the inflatable bolt. The additional friction angle of the percussive boreholes in the high-strength concrete equivalent to hard rock is approximately 5.83° . This additional friction angle,

expressing the roughness of the borehole surface, may be valid for percussively drilled boreholes in hard rock.

The tests showed that the pull load capacity increases as the installation water pressure increases in the range of 24–30 MPa. This is a preliminary conclusion that needs to be confirmed by additional work.

The observations of the frictional scratches on the surface of the bolts indicate that an inflatable bolt is anchored in the borehole in three zones along the perimeter of the bolt: the two tongue shoulders and an area opposite the tongue. The contact area was found to be the smallest in medium-sized boreholes.

Appendix: Results of Unfolding Test in the Air for Bolts B33, B34 and B35

See Figs. 24, 25, 26.

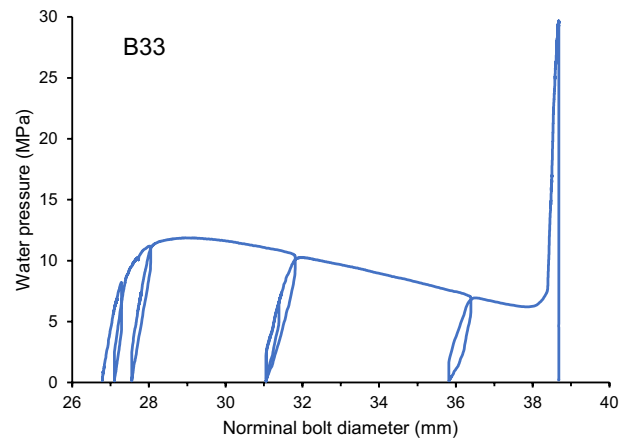


Fig. 24 The curve of water pressure against bolt diameter during the unfolding of bolt B33 in the air

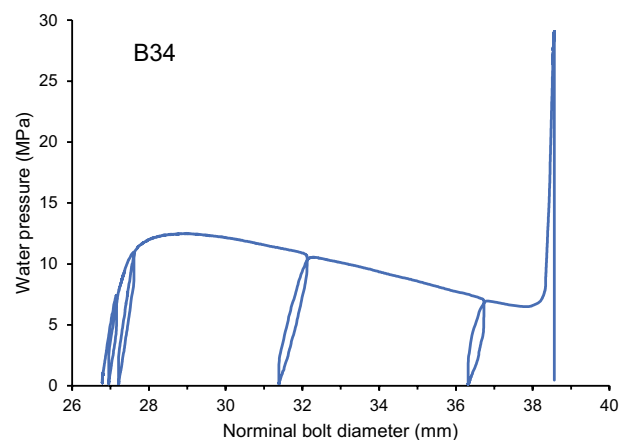


Fig. 25 The curve of water pressure against bolt diameter during the unfolding of bolt B34 in the air

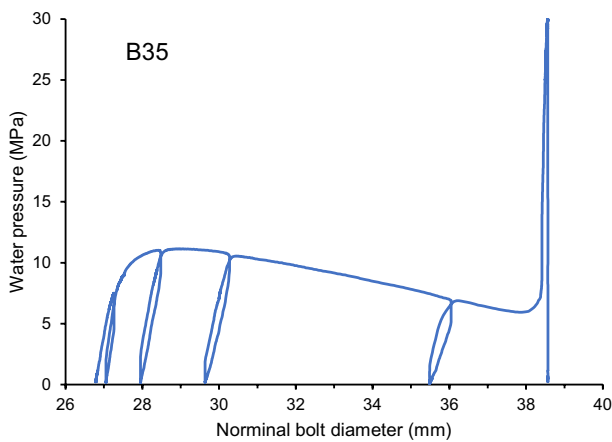


Fig. 26 The curve of water pressure against bolt diameter during the unfolding of bolt B35 in the air

Acknowledgements The authors are grateful to Gunnar Vistnes and Jon Runar Drotninghaug for their assistance with the laboratory tests.

Funding Open access funding provided by NTNU Norwegian University of Science and Technology (incl St. Olavs Hospital - Trondheim University Hospital).

Data availability Not applicable.

Declarations

Conflict of interest The authors have no conflict of interest to declare.

Open Access This article is licensed under a Creative Commons Attribution 4.0 International License, which permits use, sharing, adaptation, distribution and reproduction in any medium or format, as long as you give appropriate credit to the original author(s) and the source, provide a link to the Creative Commons licence, and indicate if changes were made. The images or other third party material in this article are included in the article's Creative Commons licence, unless indicated otherwise in a credit line to the material. If material is not included in the article's Creative Commons licence and your intended use is not permitted by statutory regulation or exceeds the permitted use, you will need to obtain permission directly from the copyright holder. To view a copy of this licence, visit <http://creativecommons.org/licenses/by/4.0/>.

References

- Alejano LR, Muralha J, Ulusay R, Li CC, Perez-Rey I, Karakul H, Chryssanthakis P, Aydan Ö (2018) ISRM suggested method for determining the basic friction angle of planar rock surfaces by means of tilt tests. *Rock Mech Rock Eng* 51:3853–3859
- Bjurholt J (2007) Pull and shear tests of rock bolts. Master Thesis, Luleå University of Technology, Sweden (in Swedish)

- Carranza-Torres C (2009) Analytical and numerical study of the mechanics of rockbolt reinforcement around tunnels in rock masses. *Rock Mech Rock Eng* 42(2):175–228
- Epiroc (2022) Epiroc, X-Pandabolt. <https://www.epiroc.com/en-ba/products/rock-drilling-tools/ground-support/quasi-static-rockbolts/inflatable-rockbolts/x-pandabolt>
- Grasselli G (2005) 3D behaviour of bolted rock joints: experimental and numerical study. *Int J Rock Mech Min Sci* 42(1):13–24
- Hagen SA, Larsen T, Berghorst A, Knox G (2019) Laboratory full-scale rock bolt testing: analysis of recent results. In: *Deep mining 2019: proceedings of the ninth international conference on deep and high stress mining*, 24–25 June, pp 217–230
- Håkansson U, Li CC (1997) Swellex in weak and soft rock—design guidelines. In: *International symposium on rock support—applied solution for underground structures*, 22–25 June, pp 555–568
- Jenmar (2022) M3 expandable rock bolt. <https://www.jenmar.com/products/m3-expandable-rock-bolt>
- Kim KC, Kim HJ, Jung YH, Shin JH (2017) Anchorage mechanism of inflatable steel pipe rockbolt depending on rock stiffness. *J Korean Tunnel Undergr Space Assoc* 31:249–263 (in Korean)
- Li C, Håkansson U (1999) Performance of the Swellex bolt in hard and soft rocks. In: *Proceedings of the international conference on rock support and reinforcement practice in mining*, pp 103–108
- Li CC (2016) Analysis of inflatable rock bolts. *Rock Mech Rock Eng* 49:273–289
- Li CC (2017) *Rockbolting: principles and applications*. Butterworth-Heinemann, Oxford
- Li CC, Zhang N, Ruiz J (2019) Measurement of the basic friction angle of planar rock discontinuities with three rock cores. *Bull Eng Geol Env* 78(2):847–856
- Player JR, Villaescusa E, Thompson AG (2009) Dynamic testing of friction rock stabilisers. In: *Proceedings of the 3rd Canada-US rock mechanics symposium and 20th Canadian rock mechanics symposium*
- Scolari F, Brandon M, Krekula H (2017) Dynamic inflatable, friction rockbolt for deep mining. In: *Deep mining 2017: proceedings of the eighth international conference on deep and high stress mining*, pp 763–772
- Stimpson B (1981) A suggested technique for determining the basic friction angle of rock surfaces using core. *Int J Rock Mech Min Sci Geomech Abstr* 18(1):63–65
- Soni A (2000) Analysis of Swellex bolt performance and a standardized rockbolt pull test datasheet and database. Master Thesis, University of Toronto, Canada
- SSAB (2022) SSAB ERB—expandable rock bolt for instant rock reinforcing. <https://www.ssab.com/brands-and-products/expandable-rock-bolts>
- Turner MH, Green T (2007) Inflatable Rockbolts at Otter-Juan Mine, Kambalda. In: *Deep mining 2007—proceedings of the fourth international seminar on deep and high stress mining*. Australian Centre for Geomechanics, pp 313–323
- Wijk G, Skogberg B (1982) The Swellex rock bolting system. In: *14th Canadian rock mechanics symposium*, Vancouver, British Columbia, 13–14 May, pp 106–115

Publisher's Note Springer Nature remains neutral with regard to jurisdictional claims in published maps and institutional affiliations.